J|A|C|S ARTICLES

Published on Web 04/14/2010

Constructing Hierarchical Spheres from Large Ultrathin Anatase TiO_2 Nanosheets with Nearly 100% Exposed (001) Facets for Fast Reversible Lithium Storage

Jun Song Chen,[†] Yi Ling Tan,[†] Chang Ming Li,[†] Yan Ling Cheah,[‡] Deyan Luan,[‡] Srinivasan Madhavi,[‡] Freddy Yin Chiang Boey,[‡] Lynden A. Archer,*[,§] and Xiong Wen Lou*[,†,§]

School of Chemical and Biomedical Engineering, Nanyang Technological University, 70 Nanyang Drive, Singapore 637457, School of Materials Science and Engineering, Nanyang Technological University, 50 Nanyang Avenue, Singapore 639798, and Kaust-Cornell Center for Energy and Sustainability, Cornell University, Ithaca, New York 14853

Received January 6, 2010; E-mail: laa25@cornell.edu; xwlou@ntu.edu.sg

Abstract: Synthesis of nanocrystals with exposed high-energy facets is a well-known challenge in many fields of science and technology. The higher reactivity of these facets simultaneously makes them desirable catalysts for sluggish chemical reactions and leads to their small populations in an equilibrated crystal. Using anatase TiO_2 as an example, we demonstrate a facile approach for creating high-surface-area stable nanosheets comprising nearly 100% exposed (001) facets. Our approach relies on spontaneous assembly of the nanosheets into three-dimensional hierarchical spheres, which stabilizes them from collapse. We show that the high surface density of exposed TiO_2 (001) facets leads to fast lithium insertion/deinsertion processes in batteries that mimic features seen in high-power electrochemical capacitors.

Introduction

Shape-controlled synthesis of nanocrystals with exposed high-energy/reactive facets is of great importance for both fundamental studies and technological applications (e.g., energy storage in electrochemical capacitors and catalysis) in multiple fields.[1−7] Anatase titanium oxide (TiO_2) with a tetragonal crystal structure is probably the most studied metal oxide.[8−11] The surface energies of its (001) and (101) facets have been calculated to be 0.90 and 0.44 J m^{-2}, respectively.[12] As a result, anatase nanocrystals are usually observed in a truncated bipyramidal shape dominated by energetically stable (101) facets. Although they are as likely to form during the earliest stages of crystal growth, the more reactive (001) facets are quickly eliminated.[1,12,13]

Following the first report of anatase TiO_2 microcrystals with ~47% exposed (001) facets,[14] a series of studies by research groups worldwide have demonstrated syntheses of sheetlike anatase TiO_2 single crystals with as high as 89% exposed (001) facets.[12,15−19] However, the construction of hierarchical structures from these interesting anatase TiO_2 nanosheets (NSs) has not been realized. Another observation is that despite the high percentages of (001) facets that survive crystal growth, the specific surface area of the TiO_2 bearing these facets is unacceptably low because of the relatively large crystal thickness in the [001] direction. For example, the specific surface area of anatase TiO_2 NSs (1.09 μm in width, 260 nm in thickness) with 64% exposed (001) facets is only 1.6 m^2 g^{-1}.[17]

Reducing the thickness in the [001] direction and increasing the two-dimensional lateral size of the (001) planes should result in a simultaneous increase in the percentage of exposed (001) facets and the specific surface area of sheetlike anatase TiO_2 crystals. Stucky and co-workers used this approach to synthesize anatase TiO_2 NSs with thicknesses of less than 1 nm by

[†] School of Chemical and Biomedical Engineering, Nanyang Technological University.

[‡] School of Materials Science and Engineering, Nanyang Technological University.

[§] Cornell University.

(1) Yin, Y.; Alivisatos, A. P. *Nature* **2005**, *437*, 664.
(2) Lim, B.; Jiang, M. J.; Camargo, P. H. C.; Cho, E. C.; Tao, J.; Lu, X. M.; Zhu, Y. M.; Xia, Y. N. *Science* **2009**, *324*, 1302.
(3) Tian, N.; Zhou, Z. Y.; Sun, S. G.; Ding, Y.; Wang, Z. L. *Science* **2007**, *316*, 732.
(4) Schrinner, M.; Ballauff, M.; Talmon, Y.; Kauffmann, Y.; Thun, J.; Moller, M.; Breu, J. *Science* **2009**, *323*, 617.
(5) Hu, L. H.; Peng, Q.; Li, Y. D. *J. Am. Chem. Soc.* **2008**, *130*, 16136.
(6) Lee, H.; Habas, S. E.; Kweskin, S.; Butcher, D.; Somorjai, G. A.; Yang, P. D. *Angew. Chem., Int. Ed.* **2006**, *45*, 7824.
(7) Zhu, J.; Wang, S. H.; Bian, Z. F.; Cai, C. L.; Li, H. X. *Res. Chem. Intermed.* **2009**, *35*, 769.
(8) Grätzel, M. *Nature* **2001**, *414*, 338.
(9) Schloegl, R. *Nat. Mater.* **2008**, *7*, 772.
(10) Yang, H. G.; Zeng, H. C. *Angew. Chem., Int. Ed.* **2004**, *43*, 5206.
(11) Wang, D. H.; Liu, J.; Huo, Q. S.; Nie, Z. M.; Lu, W. G.; Williford, R. E.; Jiang, Y. B. *J. Am. Chem. Soc.* **2006**, *128*, 13670.
(12) Zhang, D. Q.; Li, G. S.; Yang, X. F.; Yu, J. C. *Chem. Commun.* **2009**, 4381.
(13) Penn, R. L.; Banfield, J. F. *Geochim. Cosmochim. Acta* **1999**, *63*, 1549.
(14) Yang, H. G.; Sun, C. H.; Qiao, S. Z.; Zou, J.; Liu, G.; Smith, S. C.; Cheng, H. M.; Lu, G. Q. *Nature* **2008**, *453*, 638.
(15) Han, X.; Kuang, Q.; Jin, M.; Xie, Z.; Zheng, L. *J. Am. Chem. Soc.* **2009**, *131*, 3152.
(16) Liu, G.; Yang, H. G.; Wang, X.; Cheng, L.; Pan, J.; Lu, G. Q.; Cheng, H.-M. *J. Am. Chem. Soc.* **2009**, *131*, 12868.
(17) Yang, H. G.; Liu, G.; Qiao, S. Z.; Sun, C. H.; Jin, Y. G.; Smith, S. C.; Zou, J.; Cheng, H. M.; Lu, G. Q. *J. Am. Chem. Soc.* **2009**, *131*, 4078.
(18) Dai, Y. Q.; Cobley, C. M.; Zeng, J.; Sun, Y. M.; Xia, Y. N. *Nano Lett.* **2009**, *9*, 2455.
(19) Wu, B. H.; Guo, C. Y.; Zheng, N. F.; Xie, Z. X.; Stucky, G. D. *J. Am. Chem. Soc.* **2008**, *130*, 17563.

 10.1021/ja100102y

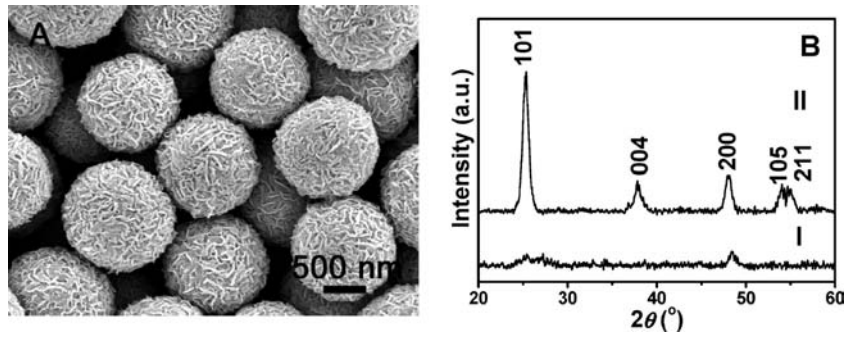

Figure 1. (A) FESEM image of the as-synthesized TiO_2 NSHSs. (B) XRD patterns of the TiO_2 NSHSs: (I) as synthesized; (II) after calcination at 400 °C.

employing a facile nonaqueous route.[19] Although bounded by the dominant (001) facets, these ultrathin TiO_2 NSs are stabilized by large amounts of oleylamine (~43 wt %) and form stacked lamellar structures. Surfactant removal by calcination to obtain pure anatase TiO_2 from the ultrathin TiO_2 NS lamellar structure is unattractive for at least two reasons: (i) it will likely lead to complete condensation and destruction of the NS, and (ii) it might promote formation of irregular, large anatase TiO_2 crystals, which would defeat the very purpose of the oleylamine stabilizing layer. One way to obtain thermally stable ultrathin NSs is to grow them into a three-dimensionally self-organized architecture, as nicely demonstrated for ultrathin zeolite NSs most recently.[20]

Herein, we report a simple synthesis of hierarchical spheres self-organized from ultrathin anatase TiO_2 NSs with nearly 100% exposed (001) facets. Several earlier studies have demonstrated that the highly reactive (001) facets of anatase TiO_2 NSs exhibit superior photocatalytic activities when normalized by the surface area.[12,15,16] Here we show that these facets also provide unusual opportunities for electrochemical energy storage. In this particular application, we have taken advantage of both the high surface activity of the synthesized anatase TiO_2 NS hierarchical spheres (TiO_2 NSHSs) and the excellent "bulk" properties imparted by their geometry. Specifically, the extremely short transport length scales in the [001] direction and a well-defined nanoporous structure facilitate fast, reversible lithium insertion/extraction, a requirement for high-power lithium ion batteries.[21,22]

Experimental Section

Materials Synthesis. In a typical synthesis, 0.03 mL of diethylenetriamine (DETA; 99%, Sigma-Aldrich) was added to 42 mL of isopropyl alcohol (IPA). After the solution was gently stirred for a few minutes, 1.5 mL of titanium(IV) isopropoxide (TIP; 97%, Sigma-Aldrich) was added. The reaction solution was then transferred to a 60 mL Teflon-lined stainless steel autoclave and kept in an electric oven at 200 °C for 24 h. It should be noted that any disturbance during the reaction (e.g., opening of the oven door) had to be avoided in order to ensure the successful formation of the desired structure. The autoclave was then taken out of the oven and left to cool naturally to room temperature. The white precipitate was harvested via centrifugation, washed thoroughly with ethanol, and dried at 60 °C overnight. All of the products were calcined at 400 °C for 2 h with a heating rate of 1 °C min^{-1} to obtain a highly crystalline anatase phase.

Materials Characterizations. The product morphology was examined using transmission electron microscopy (TEM; JEOL, JEM-2100F, 200 kV) and field-emission scanning electron microscopy (FESEM; JEOL, JSM-6700F, 5 kV). The elemental compositions of the samples were analyzed with energy-dispersive X-ray spectroscopy (EDX) attached to the FESEM instrument. Crystallographic information for the samples was collected using powder X-ray diffraction [XRD; Bruker, D8 Advance X-ray diffractometer, Cu Kα radiation (λ = 1.5406 Å)]. The surface area of the sample was measured using a Quantachrome Instruments Autosorb AS-6B instrument. For the uncalcined sample, thermogravimetric analysis (TGA) was carried out under a flow of air with a temperature ramp of 5 °C min^{-1}.

Electrochemical Measurements. The electrochemical measurements were carried out using two-electrode Swagelok cells with pure lithium metal as both the counter electrode and the reference electrode at room temperature. The working electrode consisted of active material (e.g., TiO_2 NSHSs), a conductive agent (carbon black, Super-P-Li), and a polymer binder [poly(vinylidene difluoride), PVDF, Aldrich] in a 70:20:10 weight ratio. The electrolyte used was 1.0 M $LiPF_6$ in a 50:50 (w/w) mixture of ethylene carbonate and diethyl carbonate. Cell assembly was carried out in an Ar-filled glovebox with concentrations of moisture and oxygen below 1.0 ppm. Cyclic voltammetry (1−3 V, 0.2 mV/s) was performed using an electrochemical workstation (CHI 660C). The charge/discharge tests were performed using a NEWARE battery tester at different current rates (1 C = 170 mA g^{-1}) with a voltage window of 1−3 V.

Results and Discussion

Our anatase TiO_2 NSHSs (Figure 1A) were obtained by calcining the solvothermally synthesized amine-stabilized TiO_2 NSHSs at 400 °C in static air (see the Experimental Section). The high crystallinity and phase purity of the resultant material were confirmed by XRD (Figure 1B). All of the identified peaks (pattern II in Figure 1B) can be perfectly indexed to anatase TiO_2 (JCPDS card no. 21-1272; space group $I4_1/amd$; a_o = 3.7852 Å, c_o = 9.5139 Å). The pristine uncalcined TiO_2 NSHSs were poorly crystalline in the anatase phase, as shown by pattern I in Figure 1B, in which the two weak peaks located at 2θ = 25 and 48° can be attributed to anatase (101) and (200) diffractions, respectively. TGA (Figure 2) and CHN elemental analysis revealed that they contained ~21 wt % of organic species, while the weight loss of ~12 wt % below 100 °C in Figure 2 could be attributed to the evaporation of adsorbed moisture or gaseous contents in this highly porous material (see below).

The morphology of the as-obtained anatase TiO_2 NSHSs was characterized by FESEM and TEM, as shown in Figure 3. It is immediately apparent that the spheres are quite uniform, with an average size of ~1 μm (Figure 3A,C). In the high-

(20) Choi, M.; Na, K.; Kim, J.; Sakamoto, Y.; Terasaki, O.; Ryoo, R. *Nature* **2009**, *461*, 246.
(21) Arico, A. S.; Bruce, P.; Scrosati, B.; Tarascon, J. M.; Van Schalkwijk, W. *Nat. Mater.* **2005**, *4*, 366.
(22) Kang, B.; Ceder, G. *Nature* **2009**, *458*, 190.

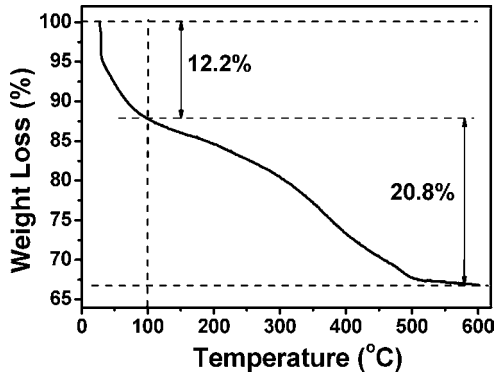

Figure 2. TGA curve of the as-synthesized TiO_2 NSHSs under an air flow at a temperature ramp of 5 °C min^{-1}.

magnification micrographs (Figure 3B,D), the constituent NSs are clearly visible and shown to adopt random orientations. The gradual contrast of the TEM image (Figure 3D) from the edge to the center of the sphere indicates that the entire sphere is indeed composed of self-organized TiO_2 NSs. The phase purity and chemical composition of the product were confirmed by EDX analysis (Figure 3E), which showed strong Ti and O signals. The self-assembly of TiO_2 NSs produces a nanoporous structure, as confirmed by the N_2 adsorption/desorption isotherm shown in Figure 3F. It gives a type-IV isotherm with a type-H3 hysteresis loop, indicating a mesoporous structure.[23] The relatively narrow pore size distributions (Figure 3F, inset) calculated using the Barrett−Joyner−Halenda (BJH) method from the two branches of the isotherm signify that most of the pores have sizes in the range 5−15 nm. Such a porous structure gives rise to a very high specific surface area of 170 m^2 g^{-1}, as calculated by the Brunauer−Emmett−Teller (BET) method.

High-resolution TEM (HRTEM) analysis was employed to determine the crystal facets. Figure 4A shows part of a single NS with visible lattice fringes. It can be observed that two sets of lattices are present and that they are oriented perpendicular to each other with an equal interfringe spacing of 0.19 nm, corresponding to anatase (020) and (200) planes. The fast Fourier transform (FFT) pattern of the same region (Figure 4A inset) can be indexed to diffraction spots of the [001] zone.[14] Therefore, it can be concluded that the TiO_2 NS is bounded by (001) facets on both the top and bottom. Figure 4C displays the HRTEM image taken from region 1 in Figure 4B (marked by a dotted circle). The distance of the visible lattice fringes over a large area was measured to be 0.19 nm, indicating that the TiO_2 NSs are single crystals when lying flat. The dark line in the TEM image (Figure 4B, region 2) demarcates the edge of a curved NS oriented approximately perpendicular to the support film. The corresponding HRTEM image (Figure 4D) also reveals lattice fringes with a distance of 0.19 nm, which is again precisely the interplane spacing of (020) and (200) facets of anatase. These dark lines can be used to estimate the thickness of the NS as only 3 nm, which explains its curved feature and high specific surface area of 170 m^2 g^{-1}. Under the assumption that each TiO_2 NS is as long as it is wide, a sheet thickness of ~3 nm and size of 100−300 nm implies that 95−99% of the exposed surfaces are (001) facets.

To understand the mechanism for formation of such a nanosheet-based hierarchical structure, different experimental conditions were investigated. Generally, no NS structures were formed using amines with other chain lengths (e.g., methylamine, ethylenediamine, oleylamine, or 1-hexadecylamine), indicating that DETA is particularly suitable and effective in producing NS-like structures in the current solvothermal synthetic system. On the other hand, TiO_2 NSs can be formed in the presence of 0.03−0.6 mL of DETA in the synthetic system. For example, when equal amounts of DETA and TIP were used (0.6 mL each), chainlike structures assembled from ultrathin TiO_2 NSs were formed (Figure 5); in these structures, the organization of the NSs was much less compact. It is hypothesized that the emerging high-energy (001) surfaces are most effectively stabilized by the tridentate DETA in the solvothermal system, which prohibits their growth along the [001] direction. After prolonged reaction, the two-dimensional lateral growth of such facets produces large ultrathin NSs. Because of their ultrathin feature, these NSs are highly flexible and thus can readily self-organize into different hierarchical architectures while still maintaining the maximized exposure of (001) facets.

Anatase TiO_2 has been intensively studied both experimentally and theoretically as the host structure for reversible lithium insertion/extraction.[24−33] The principal reaction that governs the electrochemical processes in a TiO_2/Li half-cell is thought to be

$$TiO_2 + xLi^+ + xe^- \rightleftarrows Li_xTiO_2 \quad (1)$$

with the maximum insertion coefficient x determined to be ~0.5.[34−37] This leads to a theoretical charge storage capacity of 167.5 mA h g^{-1}.[28] It is known that the diffusion of Li^+ ions in the anatase framework occurs along a reaction path connecting the vacant octahedral interstitial sites,[25,26,29] which makes diffusion more efficient along the *c* axis (i.e., in the [001] direction) than in the *ab* plane. The preponderance of accessible (001) facets in our TiO_2 NSHSs presages unusual (fast) lithium insertion/extraction kinetics.

Figure 6A displays representative cyclic voltammograms (CVs) of the anatase TiO_2 NSHSs. In agreement with previous studies, two well-defined current peaks are observed at 1.55 V (cathodic sweep) and 2.2 V (anodic sweep). The peak at 1.55 V corresponds to the biphasic transition from tetragonal anatase ($I4_1/amd$) to orthorhombic $Li_{0.5}TiO_2$ (*Imma*) when the insertion

(23) Kruk, M.; Jaroniec, M. *Chem. Mater.* **2001**, *13*, 3169.
(24) Armstrong, A. R.; Armstrong, G.; Canales, J.; Garcia, R.; Bruce, P. G. *Adv. Mater.* **2005**, *17*, 862.
(25) Lunell, S.; Stashans, A.; Ojamae, L.; Lindstrom, H.; Hagfeldt, A. *J. Am. Chem. Soc.* **1997**, *119*, 7374.
(26) Wagemaker, M.; Kentgens, A. P. M.; Mulder, F. M. *Nature* **2002**, *418*, 397.
(27) Armstrong, G.; Armstrong, A. R.; Bruce, P. G.; Reale, P.; Scrosati, B. *Adv. Mater.* **2006**, *18*, 2597.
(28) Lou, X. W.; Archer, L. A. *Adv. Mater.* **2008**, *20*, 1853.
(29) Deng, D.; Kim, M. G.; Lee, J. Y.; Cho, J. *Energy Environ. Sci.* **2009**, *2*, 818.
(30) Das, S. K.; Darmakolla, S.; Bhattacharyya, A. J. *J. Mater. Chem.* **2010**, *20*, 1600.
(31) Ortiz, G. F.; Hanzu, I.; Djenizian, T.; Lavela, P.; Tirado, J. L.; Knauth, P. *Chem. Mater.* **2009**, *21*, 63.
(32) Cheah, S. K.; Perre, E.; Rooth, M.; Fondell, M.; Harsta, A.; Nyholm, L.; Boman, M.; Gustafsson, T.; Lu, J.; Simon, P.; Edstrom, K. *Nano Lett.* **2009**, *9*, 3230.
(33) Kavan, L.; Kalbáč, M.; Zukalová, M.; Exnar, I.; Lorenzen, V.; Nesper, R.; Graetzel, M. *Chem. Mater.* **2004**, *16*, 477.
(34) Cava, R. J.; Murphy, D. W.; Zahurak, S.; Santoro, A.; Roth, R. S. *J. Solid State Chem.* **1984**, *53*, 64.
(35) Ohzuku, T.; Kodama, T.; Hirai, T. *J. Power Sources* **1985**, *14*, 153.
(36) Kavan, L.; Grätzel, M.; Rathousky, J.; Zukal, A. *J. Electrochem. Soc.* **1996**, *143*, 394.
(37) Lindstrom, H.; Sodergren, S.; Solbrand, A.; Rensmo, H.; Hjelm, J.; Hagfeldt, A.; Lindquist, S. E. *J. Phys. Chem. B* **1997**, *101*, 7717.

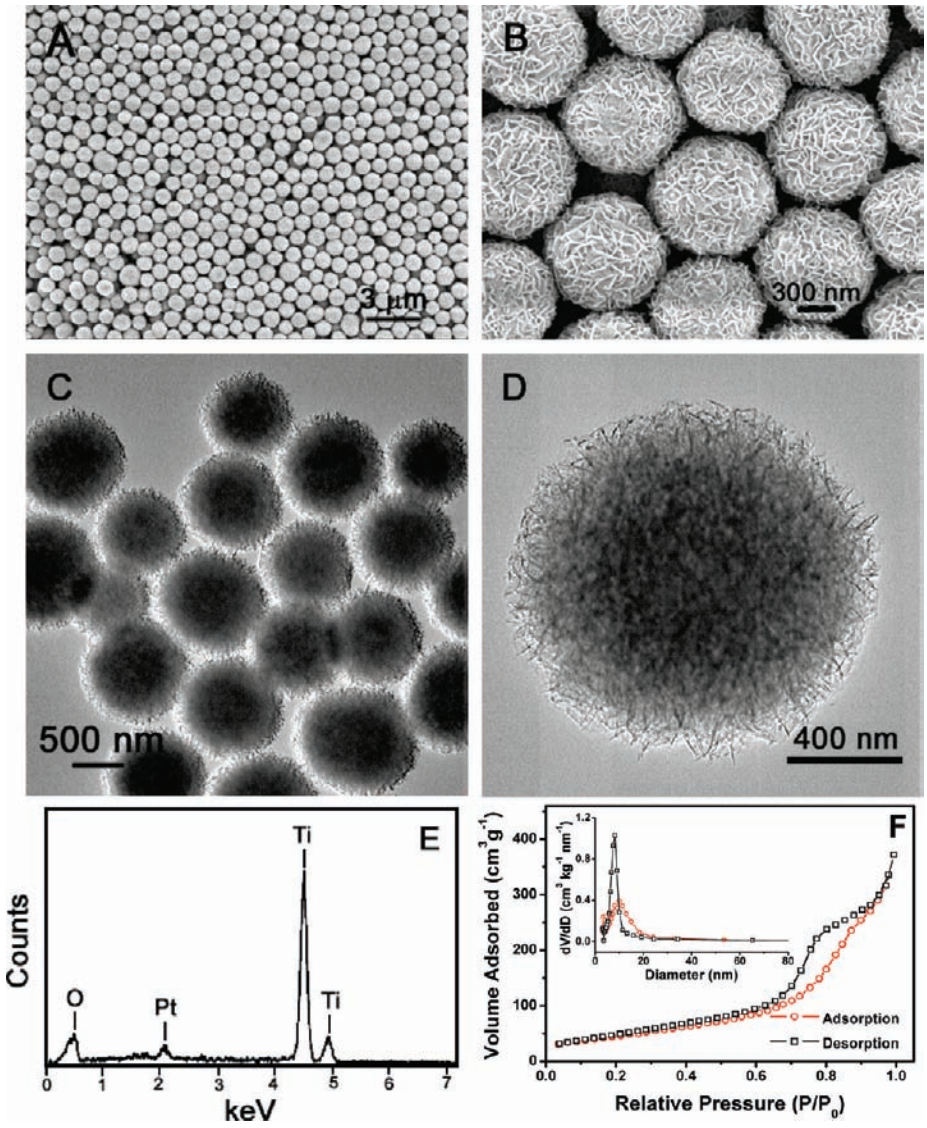

Figure 3. (A, B) FESEM images and (C, D) TEM images of as-prepared anatase TiO_2 NSHSs. (E) EDX analysis of the anatase TiO_2 NSHSs. The Pt signal arises from the Pt coating during sample preparation. (F) N_2 adsorption/desorption isotherm of the as-prepared anatase TiO_2 NSHSs. The inset shows the pore size distributions calculated using the BJH method.

coefficient x in eq 1 reaches ~0.5.[25,26,28] Interestingly, it can be observed that the intensities of both peaks increased during the subsequent scans, suggesting a possible activating process in the electrode material.[38] More strikingly, no apparent irreversible process was observed in the first cathodic scan, indicating a high Coulombic efficiency for lithium extraction. This observation is quite unusual for anatase TiO_2.

Figure 6B depicts the charge−discharge voltage profiles of the TiO_2 NSHS electrode for the first few cycles at a current rate of 5 C (850 mA g^{-1}). The results are generally consistent with the above CV analysis as well as previously reported data,[30,39] where two voltage plateaus appear at ~1.7 and ~2.1 V during the discharge and charge processes, respectively. The discharge curves clearly show that the lithium insertion process can be divided into three different stages.[39] The first stage is represented by the sharp decrease in the potential from the open-circuit voltage to a value of ~1.7 V, which is reached just before the onset of the plateau region. The next stage is the process of lithium insertion into the vacancy sites of the TiO_2 crystal structure, corresponding to the short horizontal plateau region. The final stage is the gradual decay of the voltage after the plateau region, reflecting further insertion of the lithium ions into the surface layer of the electrode material.[39] The insertion process gave a first discharge capacity of 204 mA h g^{-1} and a subsequent charge capacity of 169 mA h g^{-1}, leading to an irreversible capacity loss of only 17%. This is very low in comparison with other anatase TiO_2 electrodes, as the initial irreversible capacity loss reported is generally in the 30−40% range.[28,40−42] In the second cycle, the discharge capacity decreased to 175 mA h g^{-1} with a corresponding charge capacity of 165 mA h g^{-1}, leading to a much higher Coulumbic efficiency of 94%. This value increased further to 97% in the fifth

(38) Chen, J. S.; Lou, X. W. *Electrochem. Commun.* **2009**, *11*, 2332.
(39) Jiang, C. H.; Wei, M. D.; Qi, Z. M.; Kudo, T.; Honma, I.; Zhou, H. S. *J. Power Sources* **2007**, *166*, 239.
(40) Gao, X. P.; Lan, Y.; Zhu, H. Y.; Liu, J. W.; Ge, Y. P.; Wu, F.; Song, D. Y. *Electrochem. Solid-State Lett.* **2005**, *8*, A26.
(41) Xu, J.; Jia, C.; Cao, B.; Zhang, W. F. *Electrochim. Acta* **2007**, *52*, 8044.
(42) Song, B.; Liu, S. W.; Jian, J. K.; Lei, M.; Wang, X. J.; Li, H.; Yu, J. G.; Chen, X. L. *J. Power Sources* **2008**, *180*, 869.

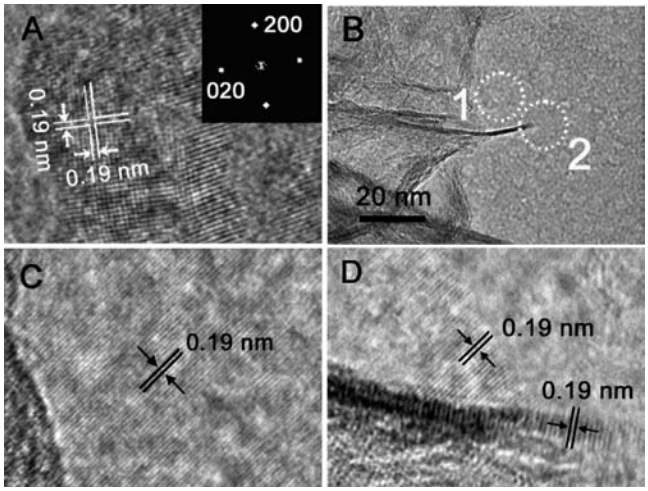

Figure 4. (A) HRTEM image of an ultrathin TiO_2 NS showing two sets of perpendicular lattice fringes with a spacing of 0.19 nm. The inset shows the FFT pattern indexed to the [001] zone. (B) TEM image recorded around the edge of a TiO_2 NS sphere. (C, D) HRTEM images of regions 1 and 2 marked with white dotted circles in (B), respectively. Both images show lattice fringes with a spacing of 0.19 nm.

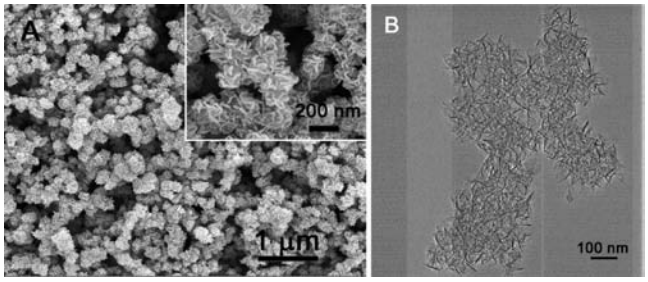

Figure 5. (A) FESEM and (B) TEM images of the chainlike structures assembled from ultrathin TiO_2 NSs (DETA and TIP, 0.6 mL each). The inset in (A) shows a FESEM image at a higher magnification.

charge−discharge cycle, indicating that the irreversible capacity loss due to trapping of Li^+ inside the TiO_2 framework decreases rapidly upon cycling.[30]

Figure 6C displays the high reversibility of the underlying electrochemical reactions over many charge−discharge cycles, at different current densities (C rates). When charged at a rate of 1 C (170 mA g^{-1}), a lithium ion battery requires ~1 h to approach its full charge capacity. Remarkably, at a rate of 1 C, a reversible capacity of 174 mA h g^{-1} was retained after more than 100 charge−discharge cycles. This corresponds to a lithium insertion coefficient of 0.52, which is slightly higher than the previously determined maximum value of 0.5. This difference is not unusual for high-surface-area nanostructures and is here attributed to the presence of an abundance of active surface sites for lithium storage.[43] As usual, the reversible capacity decreased to 136 mA h g^{-1} after 100 cycles when the C rate was increased to 5 C (850 mA g^{-1}). A further increase in the C-rate to 10 C (1700 mA g^{-1}) led to a small decrease in capacity, nicely confirming that the short diffusion path length in our ultrathin TiO_2 nanosheets leads to highly efficient solid-state diffusion of Li^+ ions. These high-rate capacities are probably among the best reported values for any TiO_2-based electrodes tested under similar conditions.

To investigate the rate capability, our TiO_2 NSHS electrode was discharged and charged at various current rates, and the

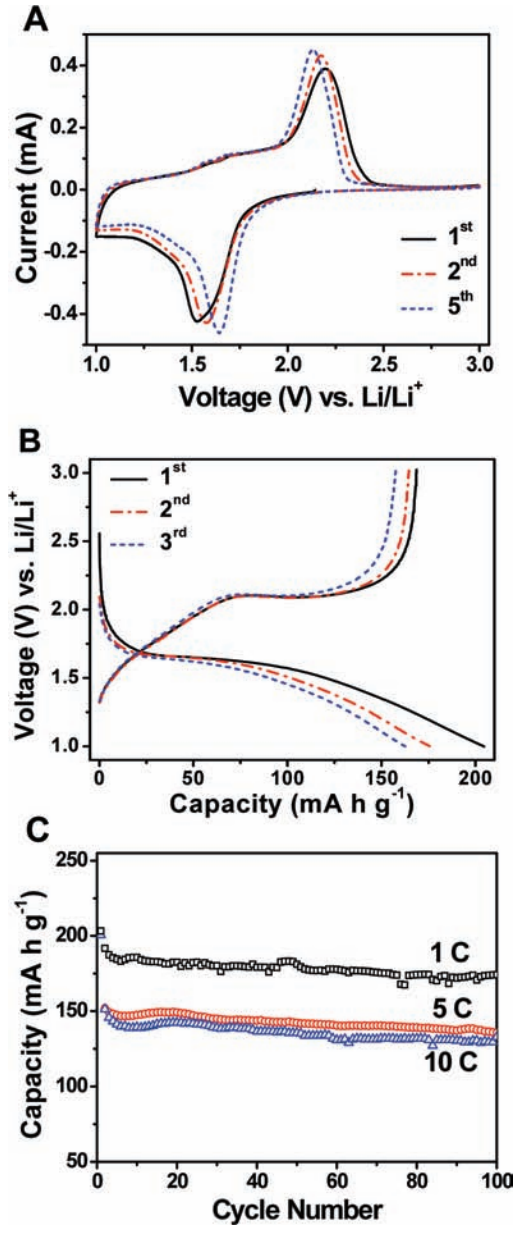

Figure 6. (A) Representative CVs at a scan rate of 0.2 mV s^{-1} for the first, second, and fifth cycles. (B) Charge−discharge profiles at a current rate of 5 C (850 mA g^{-1}) for the first, second, and fifth cycles. (C) Cycling performance at different C rates. All of the measurements were conducted using a voltage window of 1.0−3.0 V.

results are shown in Figure 7A. It can be clearly observed that our TiO_2 NSHSs show excellent capacity retention at different rates. Even at a high current rate of 20 C (3400 mA g^{-1}), a reversible capacity of 95 mA h g^{-1} could still be delivered, demonstrating a magnificent high-rate performance. Moreover, a capacity of 169 mA h g^{-1} was resumed when the rate was reduced back to 1 C. Figure 7B illustrates the current-rate dependence of the discharge capacity of the TiO_2 NSHS electrode. Apparently, the capacity decreases with increasing current density (which is equivalent to power density when multiplied by the average discharge voltage). At current rates of 0.5, 1, and 5 C, specific capacities of 224, 192, and 170 mA h g^{-1}, respectively, were obtained. It is important to mention that the first discharge capacity of 300 mA h g^{-1} could be reached at a current rate of 0.5 C, corresponding to a lithium insertion coefficient of 0.88, which is significantly higher than

(43) Guo, Y. G.; Hu, Y. S.; Maier, J. *Chem. Commun.* **2006**, 2783.

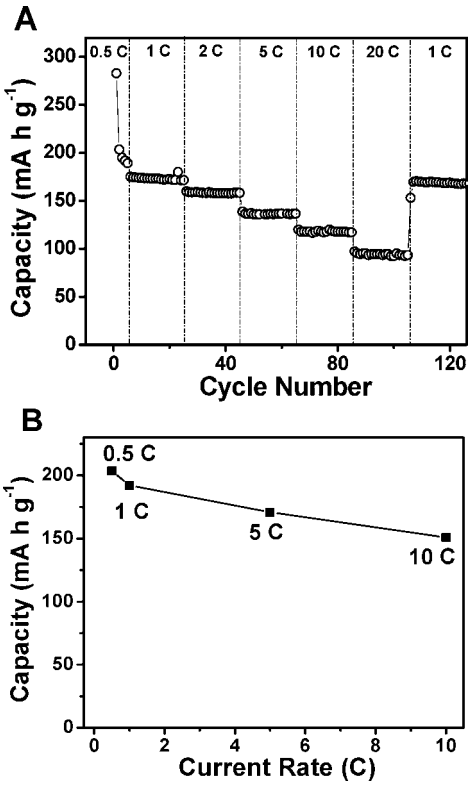

Figure 7. (A) Cycling performance of the anatase TiO_2 NSHS electrode at various charge−discharge rates. (B) Current-rate dependence of the discharge capacities of the anatase TiO_2 NSHS electrode. The capacities were extracted from the second cycle. All of the measurements were conducted using a voltage window of 1.0−3.0 V.

the theoretical value of 0.5. This high first-cycle discharge capacity is generally attributed to surface phenomena such as the irreversible decomposition of electrolyte accompanying the formation of the solid electrolyte interface (SEI)[39,43,44] as well as efficient transport of lithium ions granted by the ultrathin NSs.[30] When a current as high as 10 C (1700 mA g^{-1}) was used, our TiO_2 NSHSs were still able to deliver a reversible capacity of 150 mA h g^{-1}.

In order to further understand the enhanced lithium storage properties of these anatase TiO_2 NSHSs, we carried out post-mortem studies after 100 charge−discharge cycles at 5 C. As shown in Figure 8A,B, the overall spherical structures can be generally retained, although the detailed nanosheet structures become somewhat diminished. This is understandable, as these NSs might be too thin and large to withstand the high-rate insertion/extraction of lithium ions over extended cycling. Nevertheless, the nanosheet structure might still exist in the resulting fine particles. Our recent study showed that the nanosheet structure can be completely retained for smaller but thicker (∼10 nm) free-standing anatase TiO_2 NSs.[38] Surprisingly, the XRD analysis suggested that the anatase crystal structure can also be sustained (Figure 8C), as there was no noticeable change in the intensities of the dominant (101) peaks before and after the electrochemical test. This observation is a good demonstration of the bulk structural stability of our TiO_2 NSHSs, considering that the long-range crystal ordering of the electrode material is usually lost after extended galvanostatic cycling.[45]

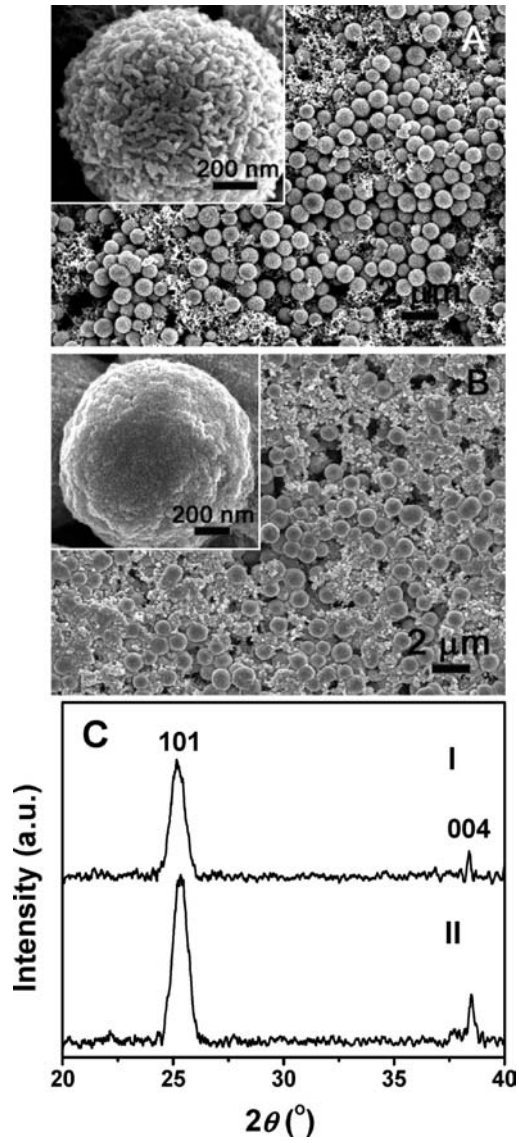

Figure 8. FESEM images of the anatase TiO_2 NSHS electrode (A) before galvanostatic discharging/charging and (B) after 100 discharge−charge cycles at 5 C (850 mA g^{-1}). The insets in (A) and (B) are magnified FESEM images of the corresponding samples. (C) XRD patterns of the samples shown in (I) panel A and (II) panel B.

Conclusions

In summary, a simple approach for synthesizing uniform hierarchical spheres self-assembled from ultrathin anatase TiO_2 nanosheets (∼3 nm in thickness and a few hundred nm in lateral size) with nearly 100% exposed (001) facets has been presented. These hierarchical spheres manifest a three-dimensional nanoporous structure with a high specific surface area of ∼170 m^2 g^{-1}. Inspired by the unique structure and inherently short transport path length of the assembled TiO_2 nanosheets, we evaluated their ability to reversibly insert/release lithium for high-power-density electrochemical energy storage in batteries. Our results show that the anatase TiO_2 NSHSs manifest an

(44) Sudant, G.; Baudrin, E.; Larcher, D.; Tarascon, J. M. *J. Mater. Chem.* **2005**, *15*, 1263.

(45) Chen, J. S.; Lou, X. W. *J. Power Sources* **2010**, *195*, 2905.

unusually high Coulombic efficiency for lithium extraction, excellent capacity retention, and superior rate behavior. In addition to their promise for use as high-power lithium ion battery electrodes, we anticipate that anatase TiO_2 nanosheet assemblies will provide long-sought-after materials solutions in multiple fields, including photocatalysis and dye-sensitized solar cells.

Acknowledgment. X.W.L. and L.A.A. acknowledge support from Award KUS-C1-018-02 made by King Abdullah University of Science and Technology (KAUST). The authors are grateful to the reviewers and Prof. Hua Chun Zeng (National University of Singapore) for very valuable comments and to Nanyang Technological University for financial support through a startup grant (SUG).

JA100102Y